Electronic Supplementary Material (ESI) for Physical Chemistry Chemical Physics.

Supplementary Materials to the manuscript "Confidence limits in pulse dipolar EPR spectroscopy: estimates for individual measurements"

Victoria N. Syryamina,[*a] Anna G. Matveeva,[*a] and Michael K. Bowman[b]

[a] *Voevodsky Institute of Chemical Kinetics and Combustion of the Siberian Branch of the Russian Academy of Science, 630090, Novosibirsk, Russia*

[b] *Department of Chemistry & Biochemistry, The University of Alabama, Tuscaloosa, AL 35487, USA*

** Corresponding authors*: *v_syryamina@kinetics.nsc.ru* (V.S.)*; matveeva@solid.nsc.ru* (A.M.)

Contents:

S1 Data Quality

Impact of truncation and sampling noise on noiseless dipolar traces

The focus of this paper is the impact of random noise. However, using data with a large time step, or coarse sampling, degrades the distance spectrum recovered by any approach; this has been called sampling noise.[1] Likewise, an experimental trace with a short length T_{max} limits the largest distance that can be recovered without degradation by truncation noise.[1,2] On the other hand, measurements with excessively short time steps or long experimental traces may not make efficient uses of limited spectrometer or cryogen resources. We verified that the dipolar trace length and sampling step used in this study do not significantly distort the distance spectrum. DL, the model-free approach with Tikhonov-based regularization, was used to recover distance spectra for dipolar traces with no random noise at different $\delta r_0/r_0$ values. DL accurately recovers the distance spectrum from the noiseless dipolar trace when $\delta r_0/r_0 < 0.15$ Fig. S1 and reasonably well even for $\delta r_0/r_0 = 0.2$.

Neither decreasing the sampling step, nor increasing the length of the dipolar trace noticeably improves the M_i parameters of the $f(r)$ at $\delta r_0/r_0 = 0.15$ and 0.2. The M_i parameters characterize the ground truth unimodal Gaussian distance distribution in terms of peak distance, peak width, and skewness as explained in the Experimental section of the paper. The DL approach recovers the distance spectrum with slightly less accuracy as $\delta r_0/r_0$ increases but there is virtually no sampling or truncation noise for the datasets used in this study. In other words, although DL shows slight biases at larger $\delta r_0/r_0$, they are not caused by sampling or truncation noise. The length and step size of the experimental trace has sufficient information for accurate recovery of the distance spectrum.

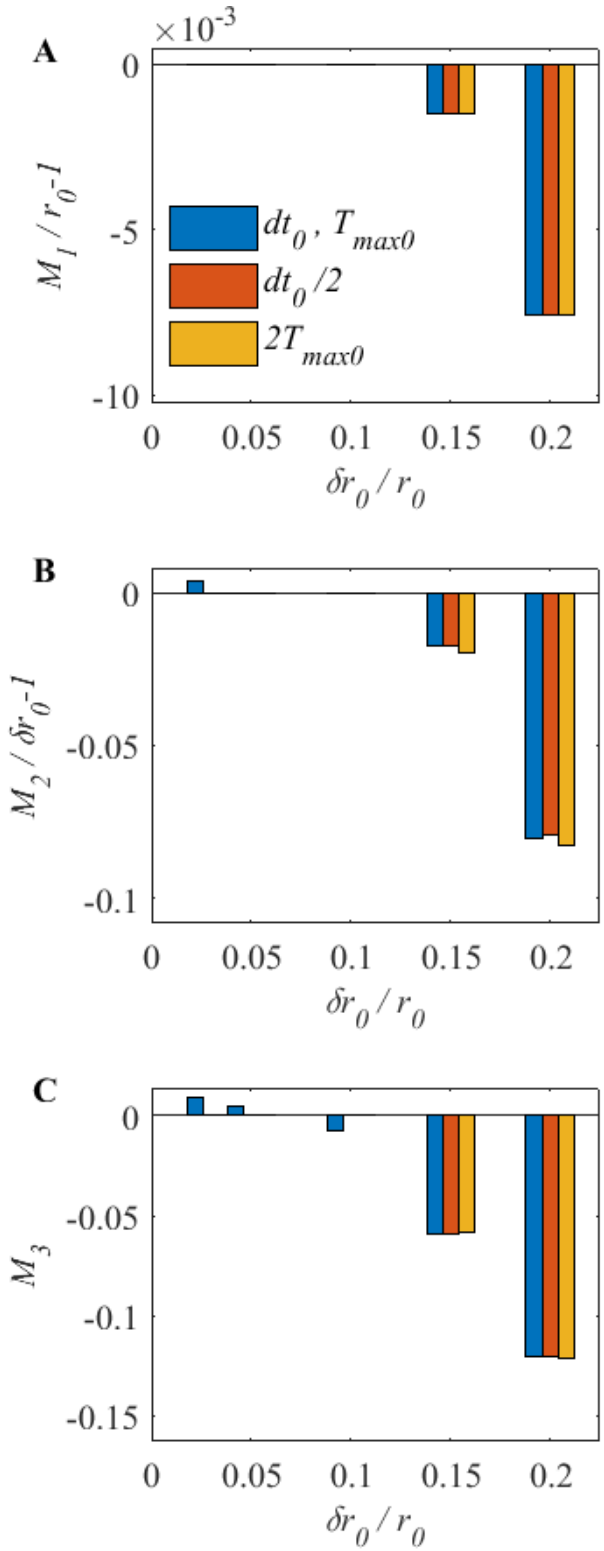

Figure S1. Impact of truncation and sampling noises on recovery of the distance spectrum from noiseless dipolar traces by the DL approach. Decreasing the time step or increasing the spectrum width has negligible impact on the recovered distance spectrum. The relative errors for M_1 (**A**), M_2 (**B**), and M_3 (**C**). The color code in panels **B** and **C** is the same as in panel **A**.

The second norm and overlap between the distance spectra and ground truth for different datasets

An objective test was used to verify that the experimental trace produces an adequate distance spectrum. The second norm Δ_2 and the overlap between the ground truth and the DL distance spectrum were calculated and compared for all datasets,[3] Fig. S2. The second norm (Euclidean norm) is the square root of the sum of squares of the residuals, which decreases with increasing SNR for all datasets, Fig.S2 A. The overlap is the sum of the minimum of the two normalized functions, which increases with increasing SNR, Fig. S2 B. Every dataset gives a consistent cluster, with a few scattered outliers.

The mean second norm does not exceed 0.02 for all datasets when SNR > 17, and the mean overlap > 0.9 for all tested datasets. Therefore, we conclude that the distance spectra evaluated by the DL approach are accurate and satisfy the conditions proposed by Schiemann et al. [3]. The traces in each dataset contain sufficient information for recovery of its distance spectrum.

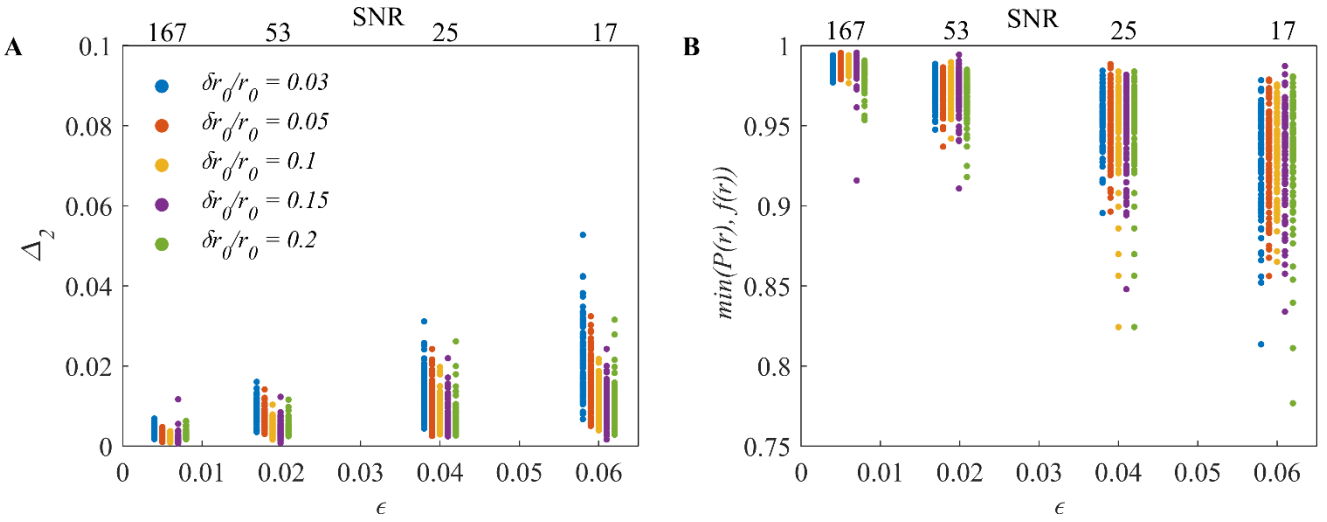

Figure S2. The second norm Δ_2 (**A**) and the overlap (**B**) between the ground truth ($P(r)$) and the distance spectrum ($f(r)$) for different datasets at different noise amplitude (bottom axis) or SNR (top axis), evaluated by the DL method.

S2 Characterization of DL distance spectra

The distance spectra were characterized for each dataset. Statistical properties were used that do not require, *a priori*, the ground truth, but do assume a unimodal Gaussian distribution for the DDF and are readily calculated for all experimental results. The characterization has two steps:

A. The first and second moments, μ_{1i} and μ_{2i} of the distribution were calculated within the open window for each $f_i(r)$. Each spectrum was 'renormalized' to give an r-distance spectrum, i.e., divided by the integral of the DDF over that spectrum's range from $\mu_{1i} - n\mu_{2i}^{1/2}$ to $\mu_{1i} + n\mu_{2i}^{1/2}$, where n = 2 or 3, or the full open window width was used. The μ_{1i}, μ_{2i} and μ_{3i} were recalculated for each r-distance spectrum over that spectrum's range.

   The relative error of $M_1 = \mu_1$, $M_2 = \mu_2^{1/2}$, and the skewness $M_{3i} = \mu_{3i}/\mu_{2i}^{3/2}$ were calculated within each spectrum's range. The range of $\mu_{1i} \pm n\mu_{2i}^{1/2}$ with n = 2 was found to provide better recovery of all parameters across all datasets, Fig. S3.

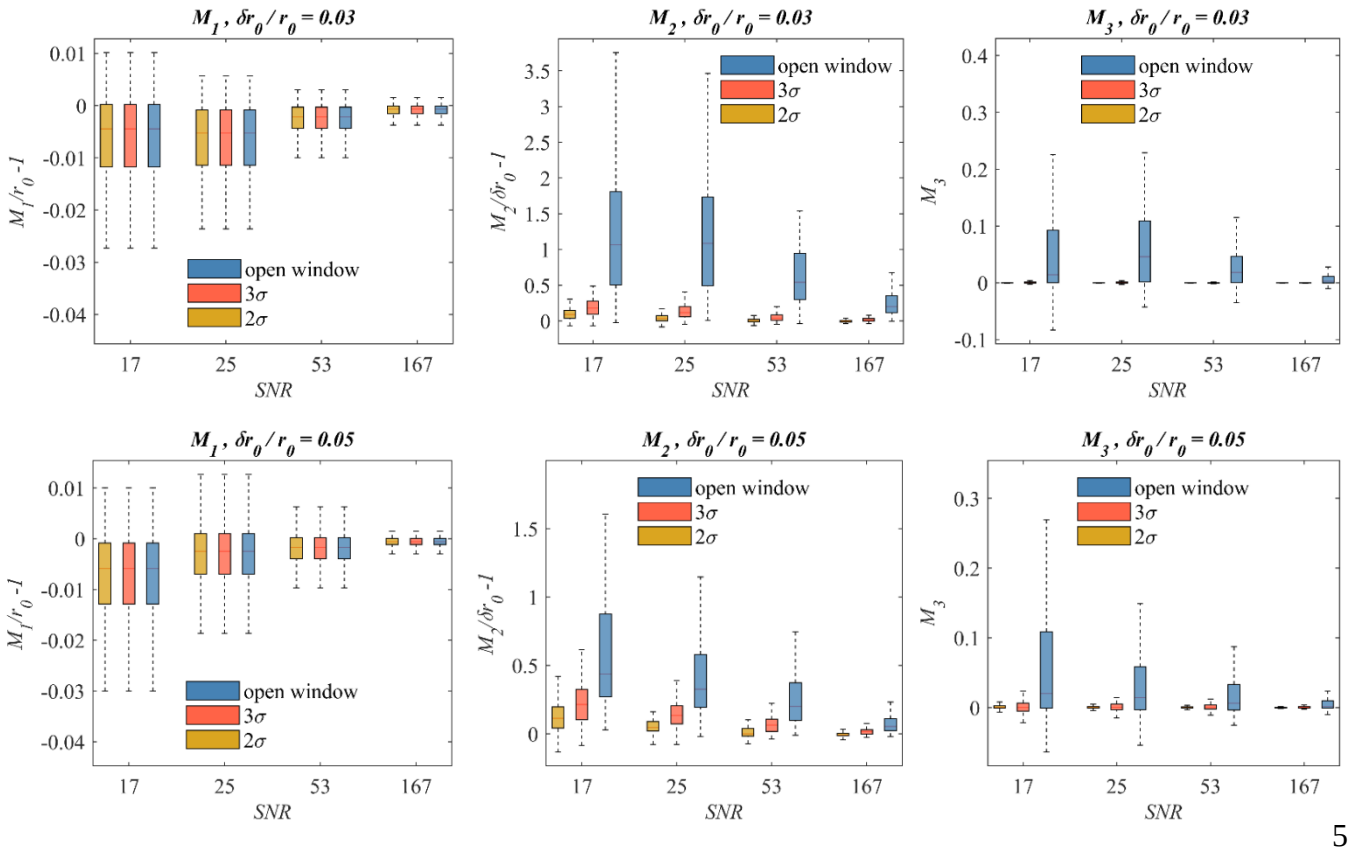

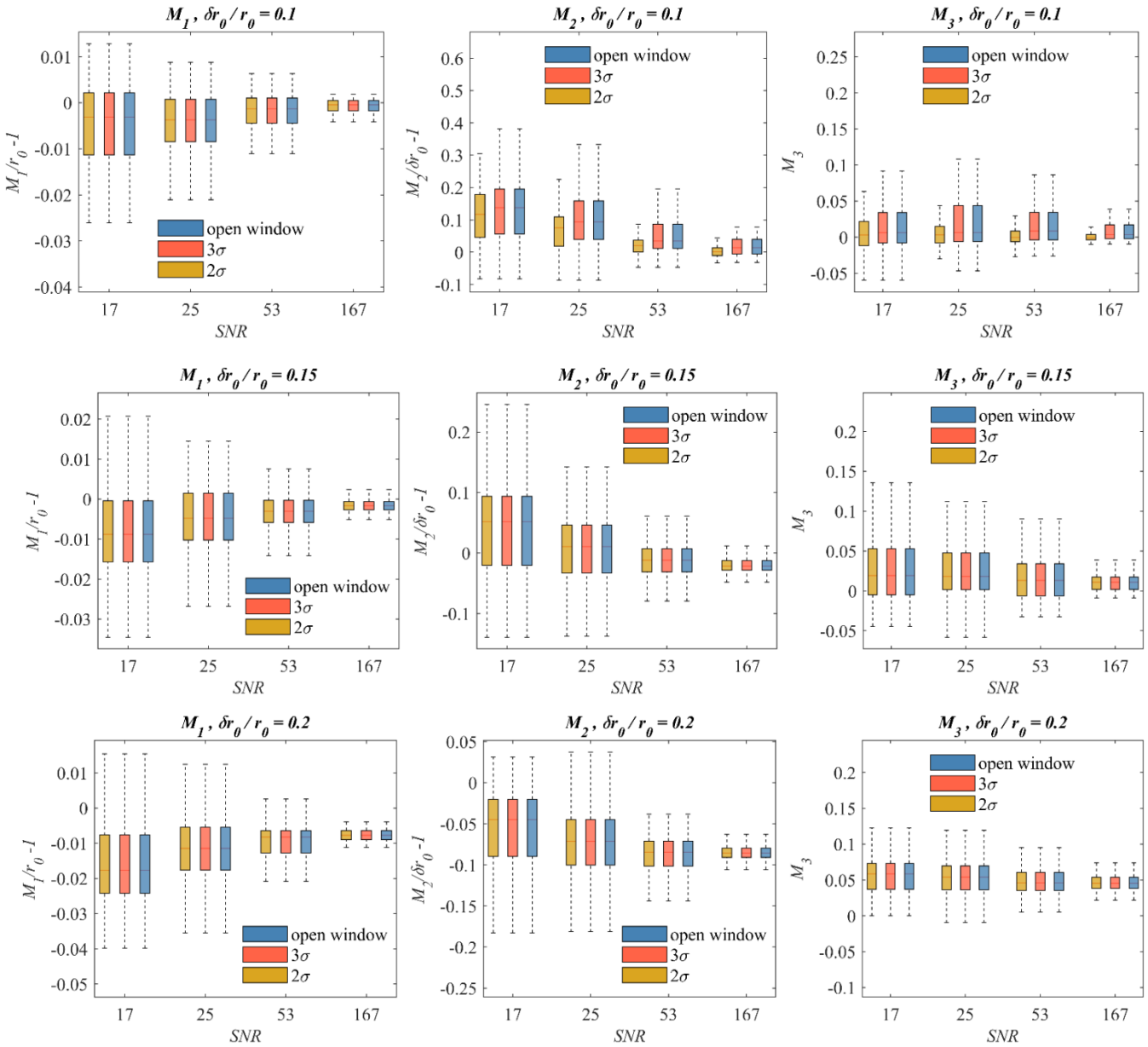

Figure S3. The relative error of M_1, M_2, and the skewness M_3 within different intervals around the peak, $\mu_{1i} \pm n\mu_{2i}^{1/2}$ with n = 2 or 3 and for the full open window, at different $\delta r_0/r_0$ and SNR values.

Each ‘renormalized’ DL distance spectrum was also fitted by a symmetric unimodal Gaussian line and its M_1, M_2 and M_3 were calculated within the $\mu_{1i} \pm 2\mu_{2i}^{1/2}$ interval, Fig. S4. This Gaussian post-processing fitting slightly improves the estimation of M_1 by less than 1% but provides mixed results with M_2. Therefore, the recovered distance spectra were characterized by M_1, M_2, and M_3 with $n = 2$.

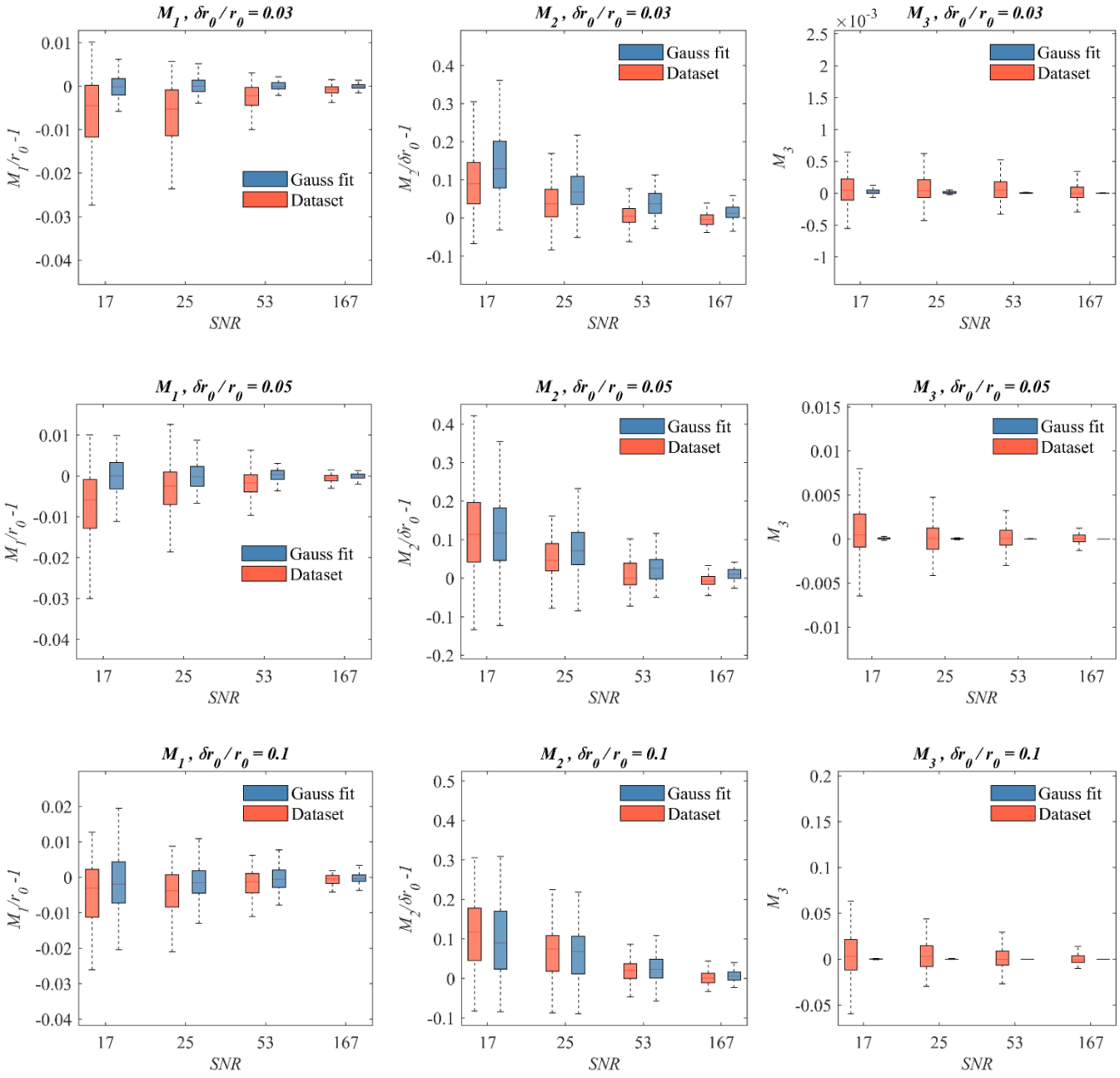

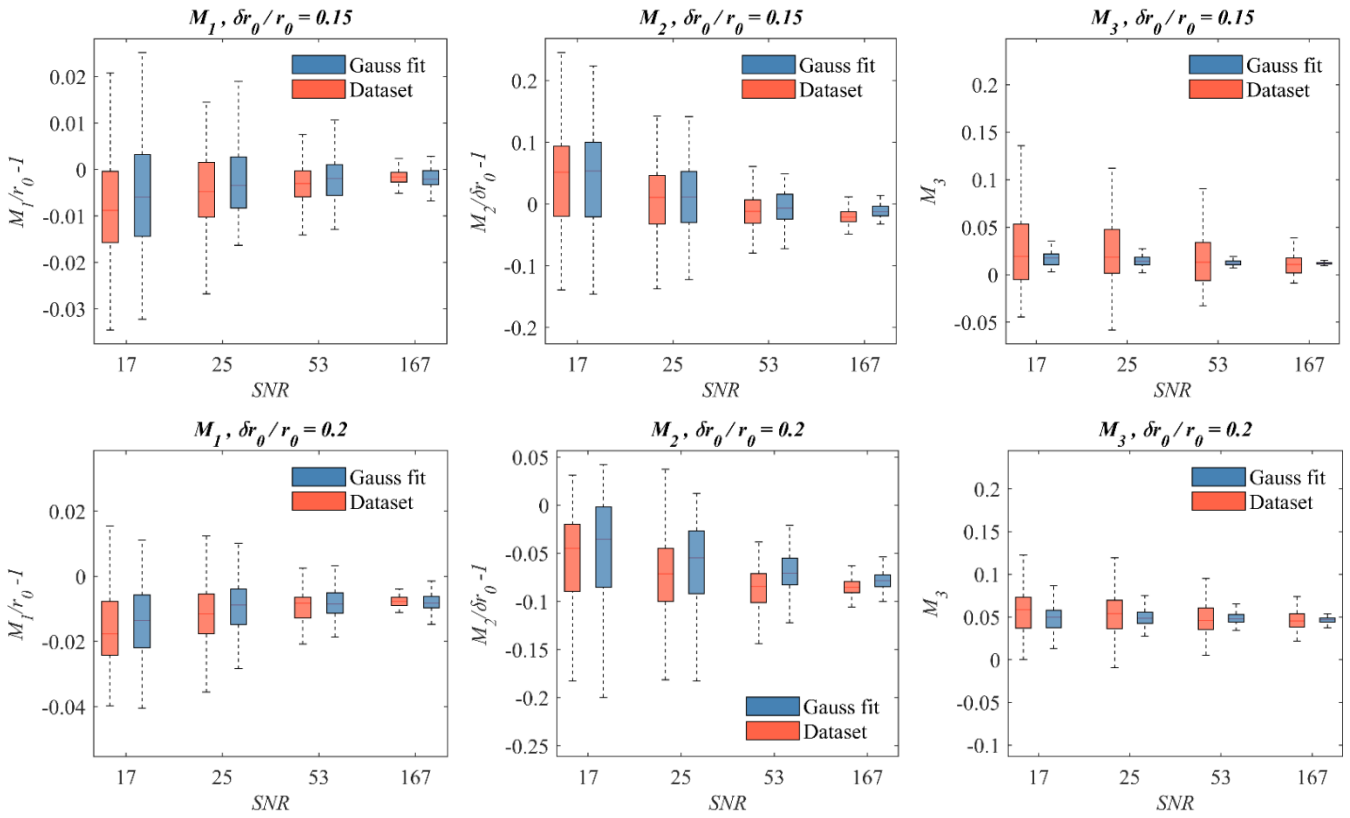

Figure S4. The relative error of M_1, M_2, and the skewness M_3 of the r-distance spectrum compared with that of a Gaussian fit of the $f(r)$ at different $\delta r_0/r_0$ and SNR values.

S3 Characterization of MeTA distance spectra

One feature of MeTA is its additivity in transforming the signal and noise from the time-domain into the distance domain.[4] This additivity can reveal how noise at different times in the experimental trace propagates into the distance spectrum. The noise at early times produces strong oscillations in the distance spectrum at short distances, Fig. S5, and decreases at larger r, as discussed previously.[1] The parameter N_τ in the Mellin transform restricts noise propagation into the distance domain (with other parameters of the Mellin transform fixed) and serves as a regularization parameter. The N_τ was optimized for noiseless traces in each dataset by the "L-curve", using the *mse* in the time domain between the noiseless dipolar trace and the trace calculated from the recovered MeTA distance spectrum, Fig. S6. However, even for the optimal N_τ, the distance spectrum has strong oscillations around the DDF at short distances, Fig. S5, which increase linearly with the noise amplitude. The distance spectrum $f(r)$ approximates the probability density, *i.e.*, the distance distribution function DDF, which should be non-negative. Therefore, for data analysis of our unimodal Gaussian distribution, we restrict the spectral range by the following steps so that the distance spectrum is non-negative:

A. Selection of the spectral range for data analysis.
    a. A lower boundary r_{cut_st} is determined as the last distance from the "left" side of the peak, at which the distance spectrum $f(r) \geq 0$.
    b. An upper boundary r_{cut_f} is determined as the maximal r, on the "right hand" side of the peak at which $f(r) \geq 0$.
    c. The f(r) within the r_{cut_st} - r_{cut_f} range is verified to be continuous.
B. The integral of $f(r)$ over the spectral range is 'renormalized' to unity (μ_{0i} = 1, r-distance spectrum).

C. The first, the second, and the third moments (μ_{1i}, μ_{2i}, μ_{3i}) of the *r*-distance spectrum and the subsequent $M_1 = \mu_1$, $M_2 = \mu_2^{1/2}$, and the skewness $M_{3i} = \mu_{3i}/\mu_{2i}^{3/2}$. M_1 and M_2 were also calculated for a Gaussian fit to each renormalized distance spectrum.

An example of a distance spectrum and its spectral range for data analysis is given in Fig. S5.

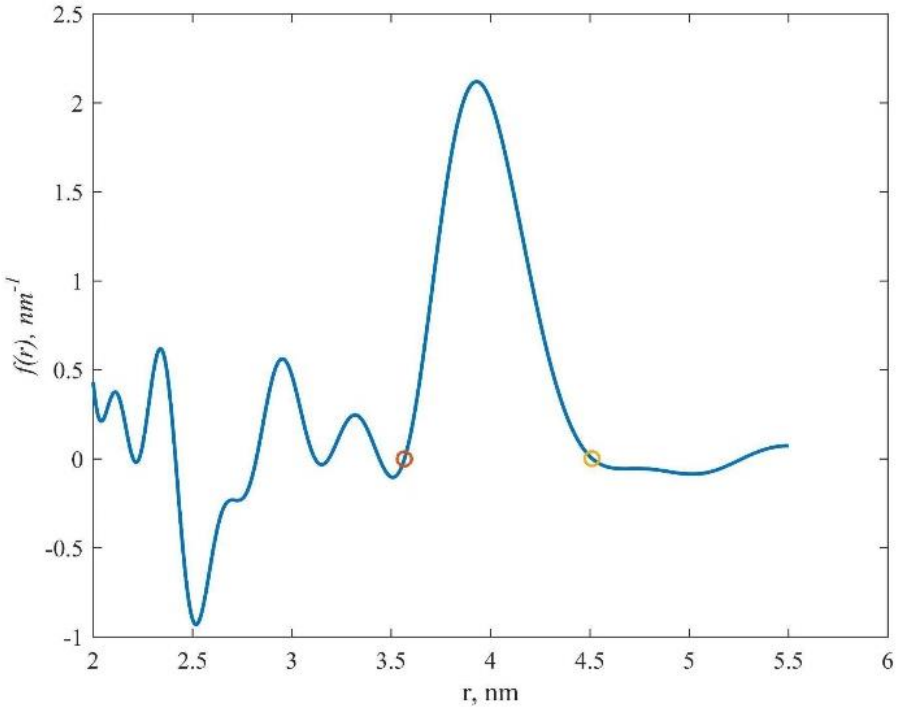

Figure S5. An example of a distance spectrum at $\delta r_0 / r_0 = 0.1$, $\epsilon = 0.06$ (SNR 17) with the red and yellow circles showing the upper and lower boundaries of the spectral range for line shape analysis.

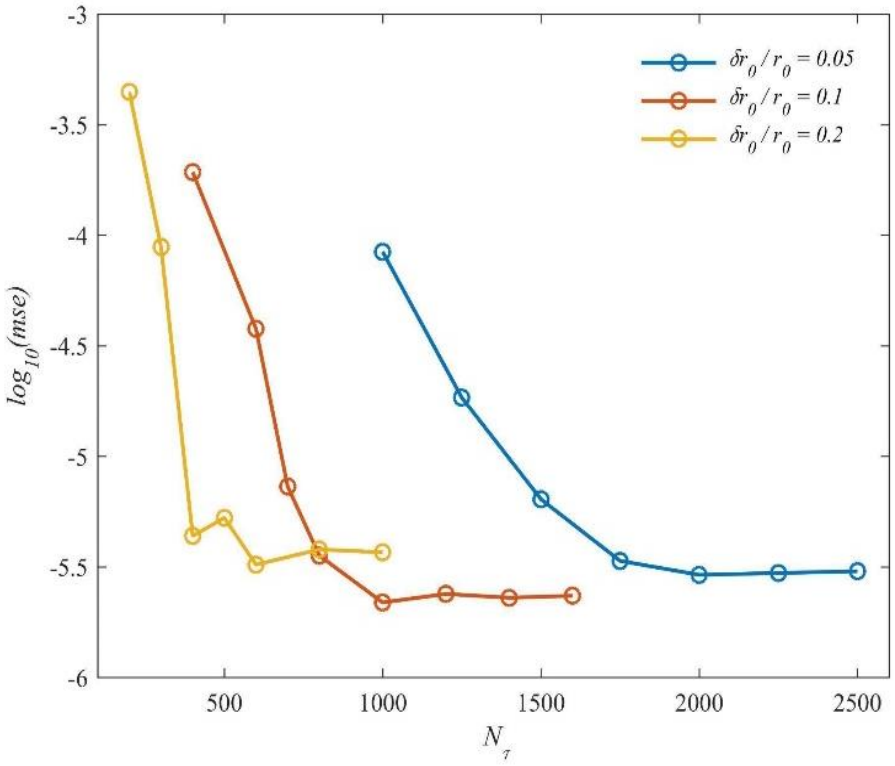

Figure S6. L-curves for optimization of the regularization parameter N_τ for noiseless traces at different $\delta r_0/r_0$ values.

For each $f(r)$, the M_{1i}, M_{2i} and M_{3i} were calculated within its optimal window either directly as $M_{1i}=\mu_{1i}$, $M_{2i}=\mu_{2i}^{1/2}$, and $M_{3i} = \mu_{3i}/\mu_{2i}^{3/2}$, or by fitting a symmetric unimodal Gaussian line to the spectrum and using its M_1 and M_2, Fig. S7. This Gaussian post-processing fitting just slightly improves the estimation of M_1 and provides mixed results with M_2. Therefore, the recovered distance spectrum was characterized by its M_1, M_2, and M_3.

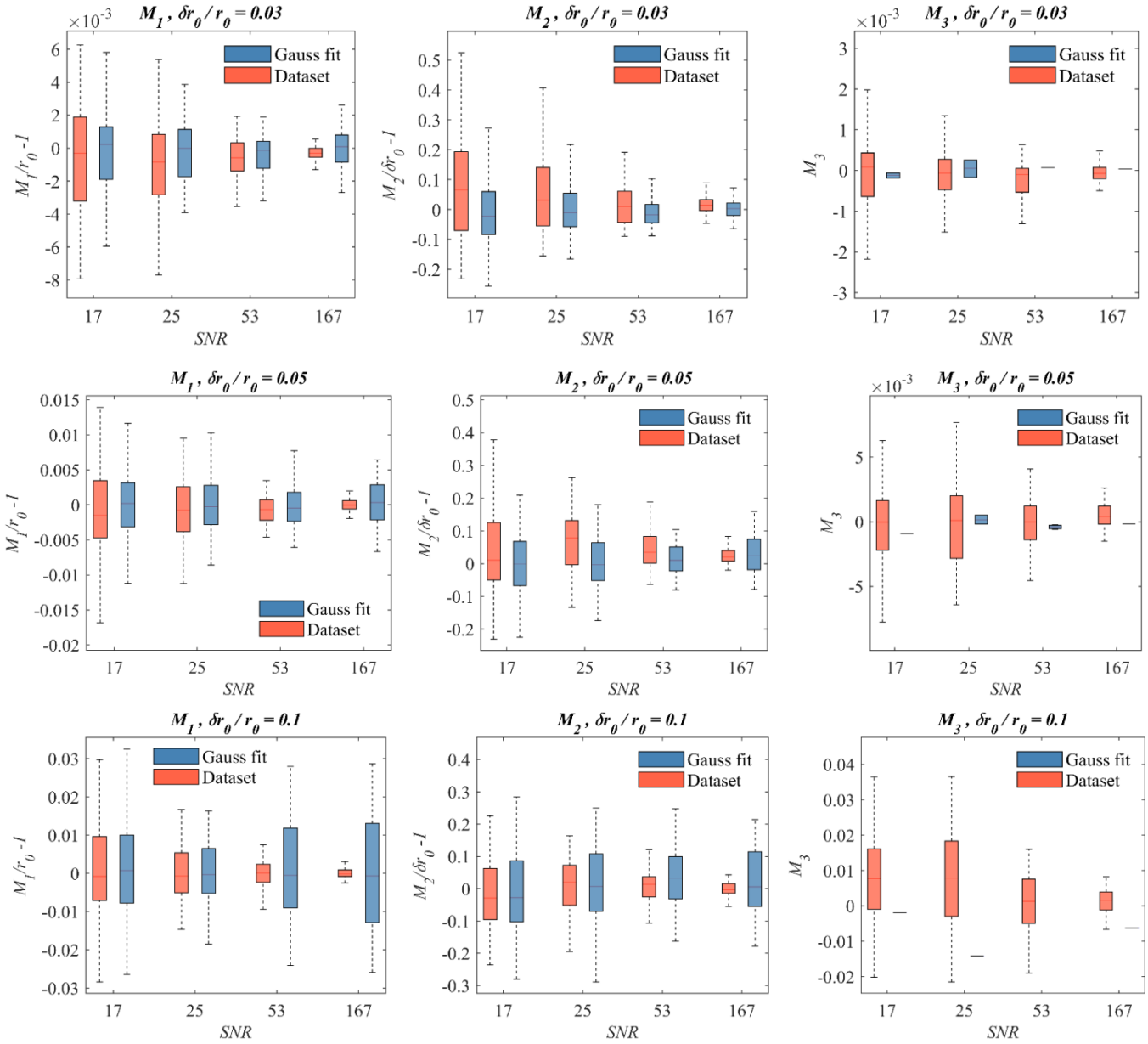

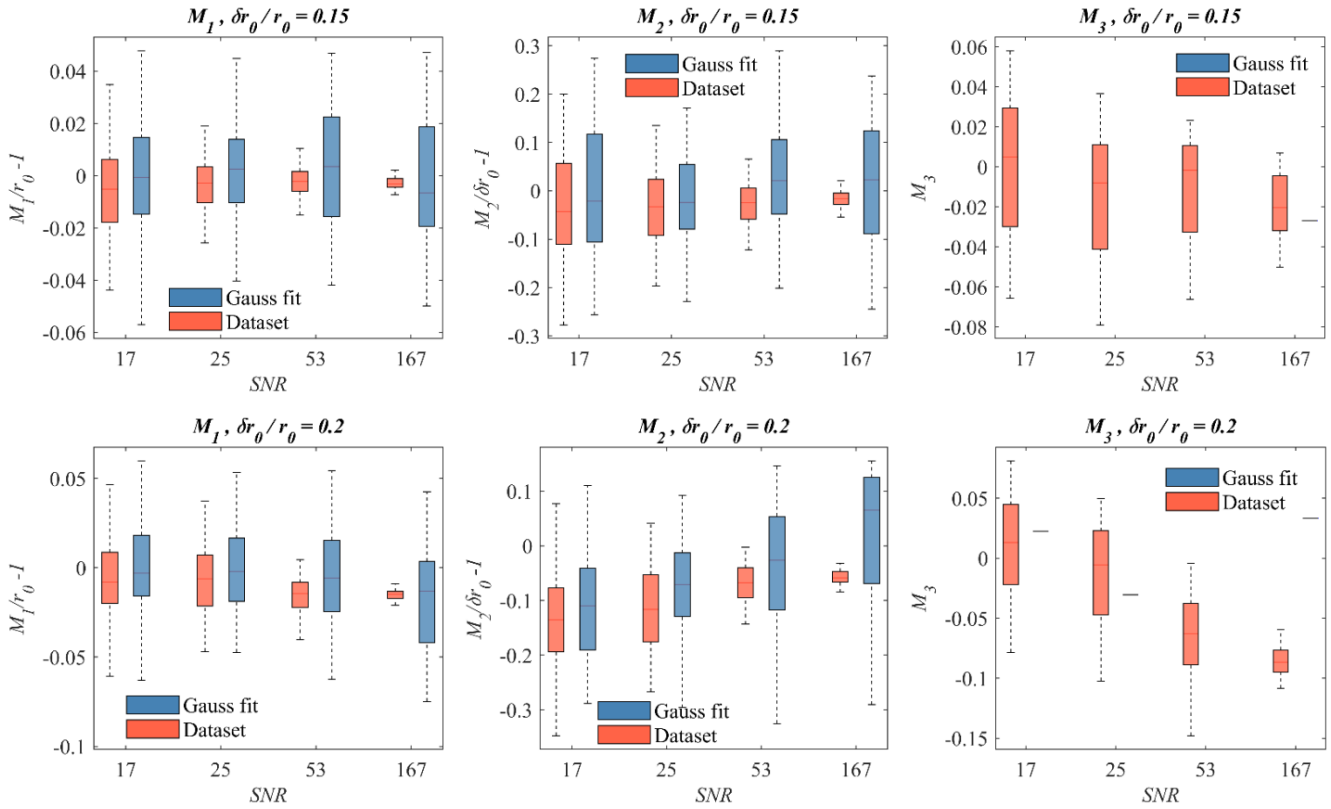

Figure S7. The relative error of M_1, M_2, and the skewness M_3 of the r-distance spectrum compared with the M_1 and M_2 of a Gaussian fit to the $f(r)$, for different $\delta r_0/r_0$ and SNR values.

S4 Comparison of results from DL, MeTA and MB

Box plots of M_1, M_2, M_3

The M_{1i}, M_{2i} and M_{3i} were calculated as $M_{1i}=\mu_{1i}$, $M_{2i}=\mu_{2i}^{1/2}$, and $M_{3i}=\mu_{3i}/\mu_{2i}^{3/2}$, for each *r*-distance spectrum obtained by DL, MB, and MeTA within its optimal window, Fig. S8. The parameters most relevant to a unimodal Gaussian distribution are M_1 and M_2. All three approaches perform well for distributions with moderate width and great SNR. DL is rather robust and works well with poor SNR, while MeTA tends to have lower bias but its uncertainty increases quickly as SNR worsens.

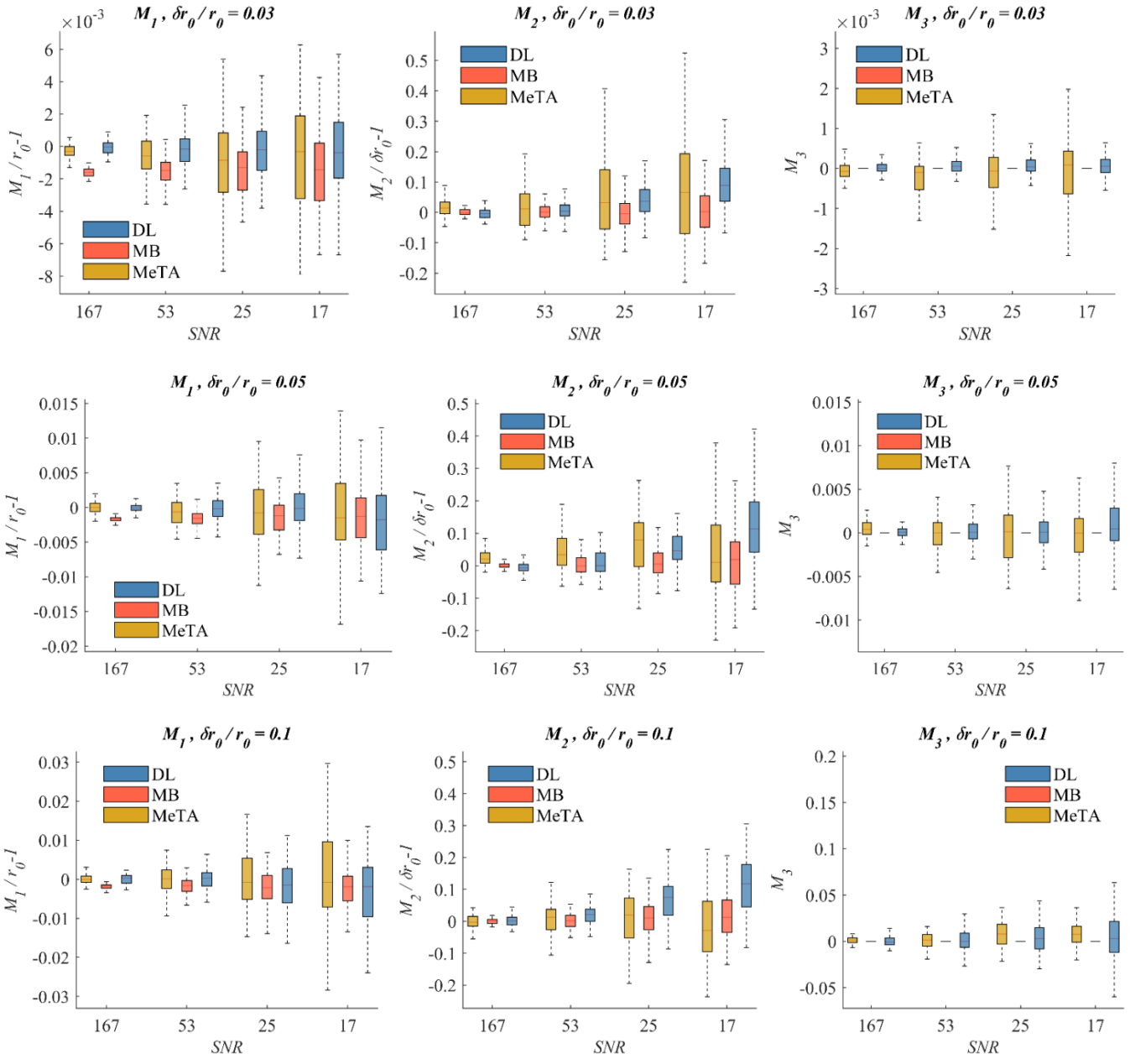

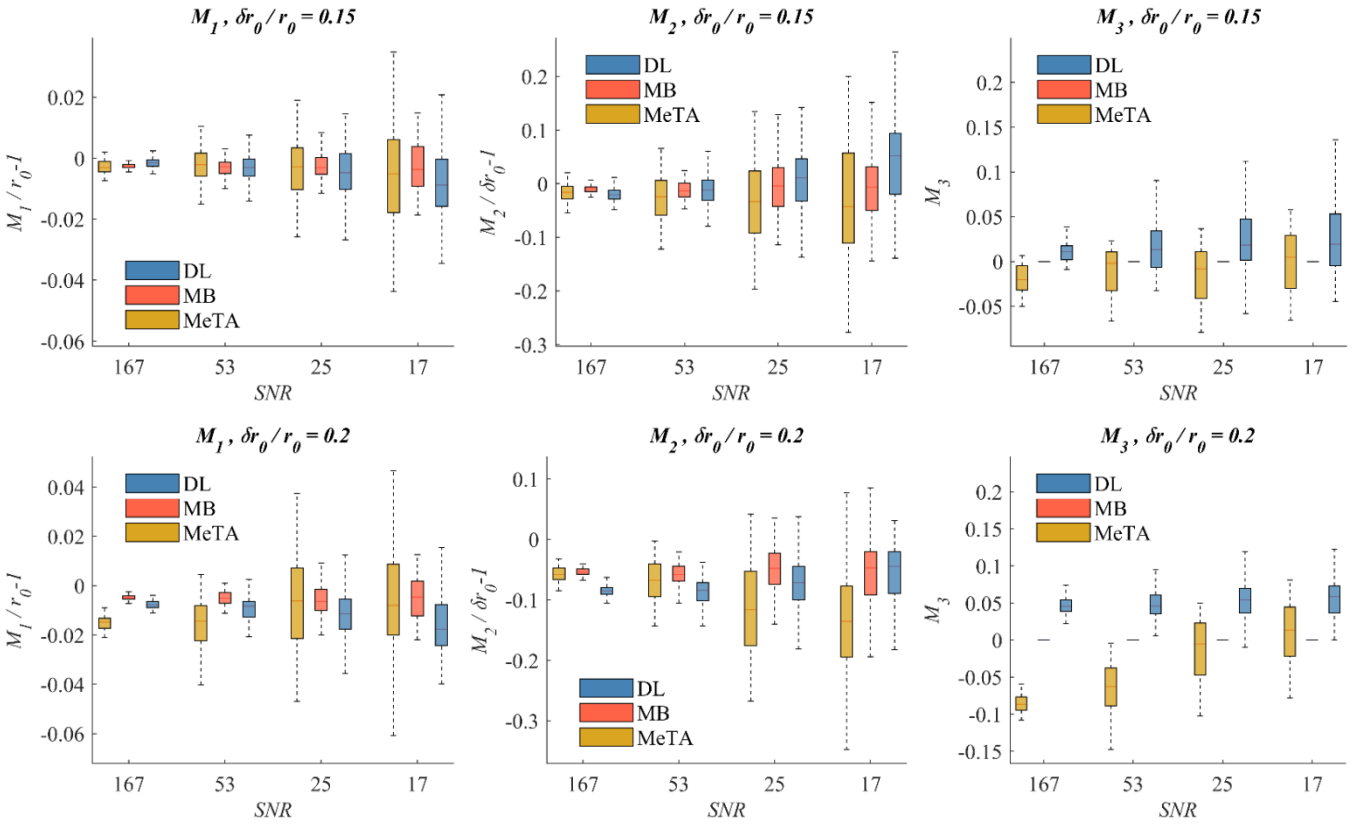

Figure S8. The relative error of M_1, M_2, and the skewness M_3 obtained by DL, MB, and MeTA at different $\delta r_0/r_0$ and SNR values.

The mean skewness for DL and MeTA

The mean skewness M_3 in the datasets treated by DL or MeTA is presented as a heatmap, Figure S9. Positive skewness means that the distance spectrum is more intense at, or skewed toward, longer distances than shorter distances. DL has a definite tendency to overestimate the intensity of the distance spectrum at large distances for broad distributions. MeTA also has significant tendencies to overestimate distance spectra at larger distances at low SNR, and to overestimate distance spectra at short distances for broad distributions at great SNR. This latter effect is somewhat puzzling because one reasonably expects more accurate results when the SNR is large. But this trend may be an unintended artifact caused by the way the distance spectra were truncated for calculation of the moments, particularly the skewness.

Calculation of the moments stops when the distance spectra become negative due to noise. So with the broad spectra, the tails of the peak extend to very short and to very long distances until finally the random noise makes them go negative and the moment calculation is halted. One would expect this to happen at the about the same distance from the peak center, with no effect on skewness. However, Figs. 1B and S5 show some sampling noise at the shortest distances with MeTA. Positive intensity in that sampling noise will be included in the skewness calculation for the broadest distributions with the best SNR, producing the negative skewness. Higher levels of random noise make the distance spectrum become negative closer to the peak, preventing most of the sampling noise from contributing to the excessive skewness. Since this occurs mainly in the extreme corner of our grid and because skewness is not a very useful property, there seems no need to eliminate this inconsequential artifact.

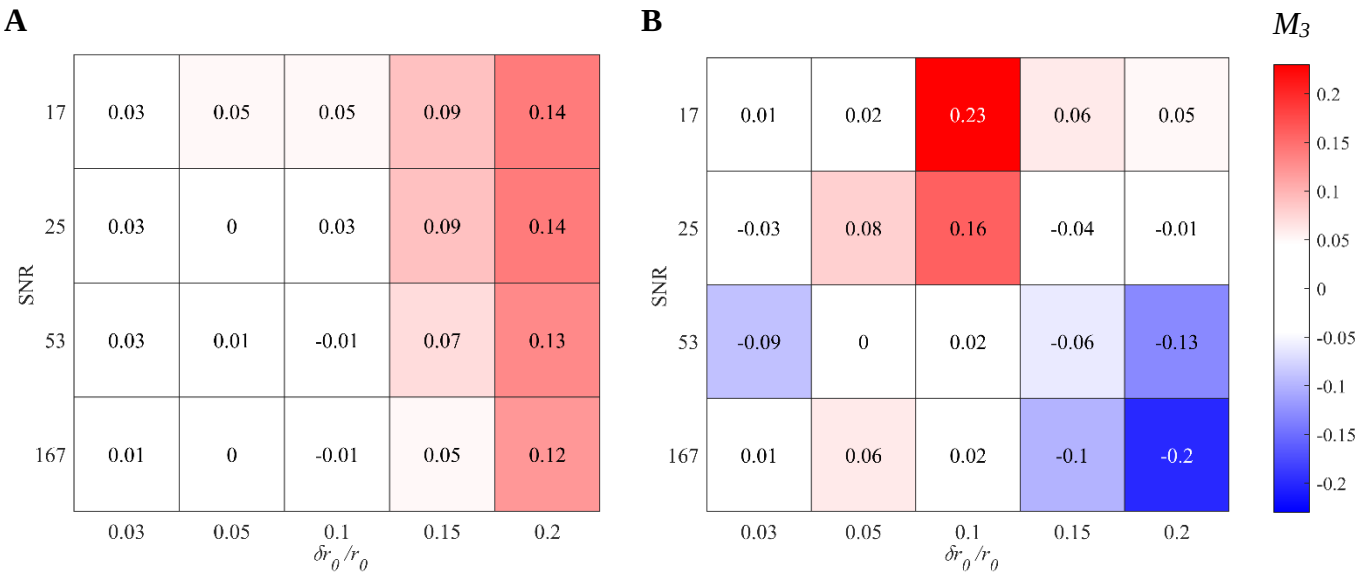

Figure S9. The mean skewness (M_3) for datasets evaluated by DL (**A**) and MeTA (**B**).

S5 Correlated Errors and Confidence Estimates

Confidence ellipses and scatter plots

Scatter plots of the relative errors in $M_1/r_0 - 1$ and $M_2/\delta r_0 - 1$ with 95% confidence ellipses were prepared for each dataset. The plots show that for moderate to broad distributions, the relative errors in M_1 and M_2 are negatively correlated, i.e., tending to overestimate one while underestimating the other. Such a correlation of errors is readily overlooked in the boxplots in sections ***S2*** and ***S5.***

These plots also reveal that some ellipses do not cover the ground truth lying at the intersection of the plot axes, meaning that the bias is large relative to the uncertainty. Fortunately, the bias often would be insignificant in the context of the nanostructures being measured. All approaches show noticeable biases for broad distributions ($\delta r_0/r_0 \geq 0.1$), but physically insignificant biases for narrower distributions and SNR >25.

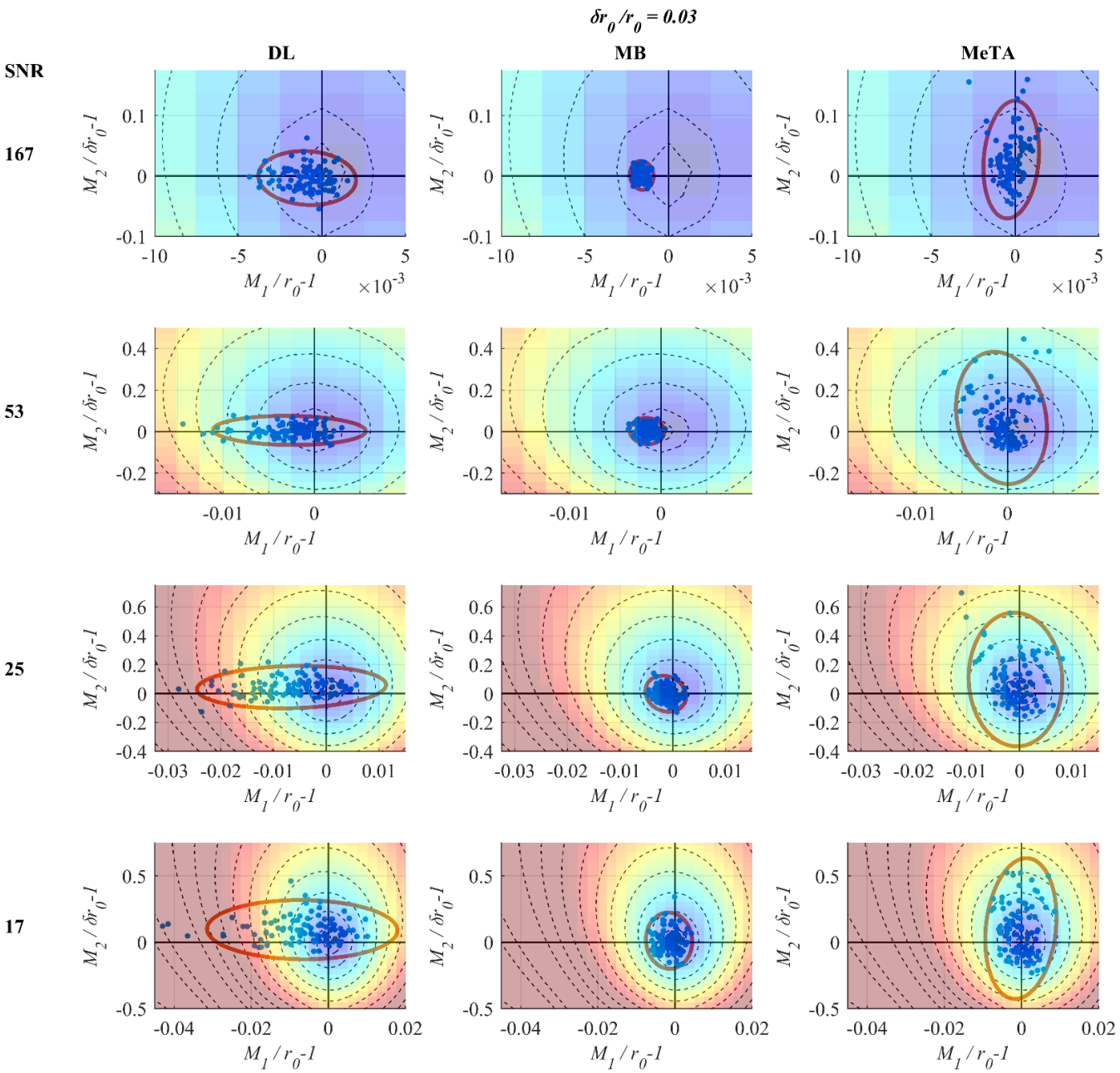

Figure S10. A scatter plot of the relative errors in the M_1 and M_2 values, evaluated by DL (left panels), MB (central panels), and MeTA (right panels) at SNR = 167, 53, 25, and 17 (from top to bottom). The red ellipses show the footprint with the CI=95%. The colored background and dashed lines show the noiseless error-surface. The width of the distance distribution is $\delta r_0/r_0 = 0.03$.

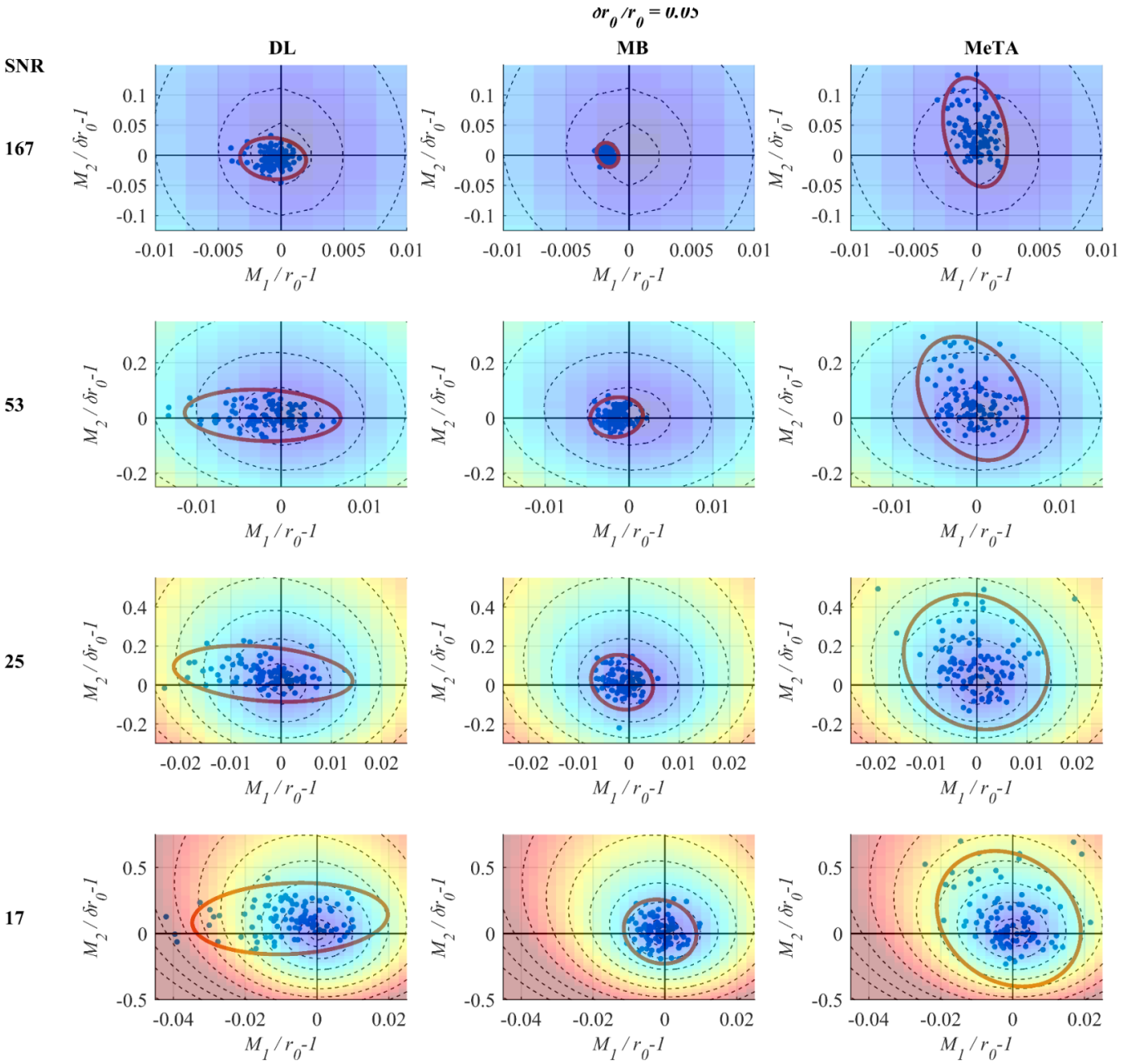

Figure S11. A scatter plot of the relative errors in the M_1 and M_2 values, evaluated by DL (left panels), MB (central panels), and MeTA (right panels) at SNR = 167, 53, 25, and 17 (from top to bottom). The red ellipses show the footprint with the CI=95%. The colored background and dashed lines show the noiseless error-surface. The width of the distance distribution is $\delta r_0/r_0 = 0.05$.

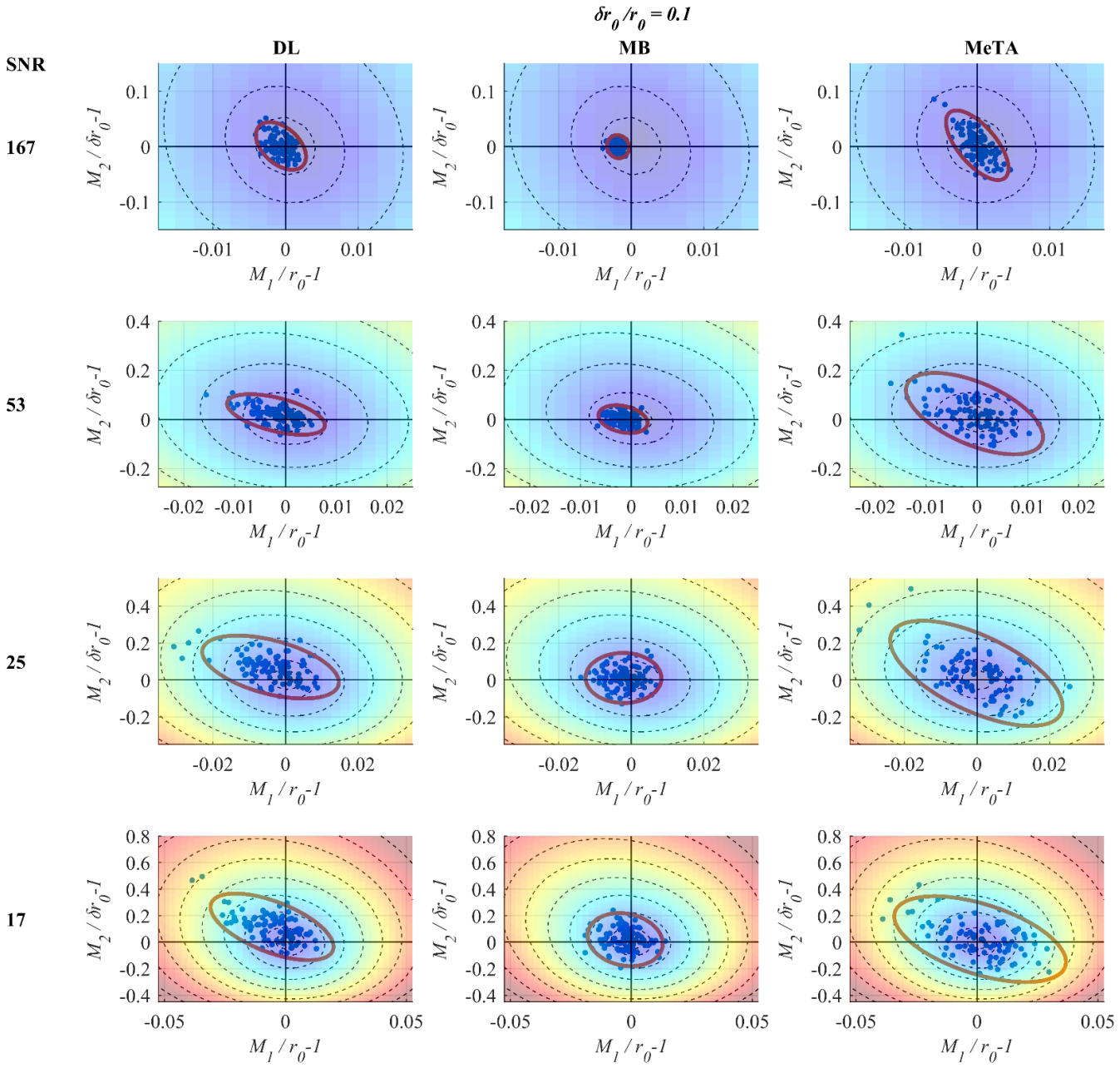

Figure S12. A scatter plot of the relative errors in the M_1 and M_2 values, evaluated by DL (left panels), MB (central panels), and MeTA (right panels) at SNR = 167, 53, 25, and 17 (from top to bottom). The red ellipses show the footprint with the CI=95%. The colored background and dashed lines show the noiseless error-surface. The width of the distance distribution is $\delta r_0/r_0 = 0.1$.

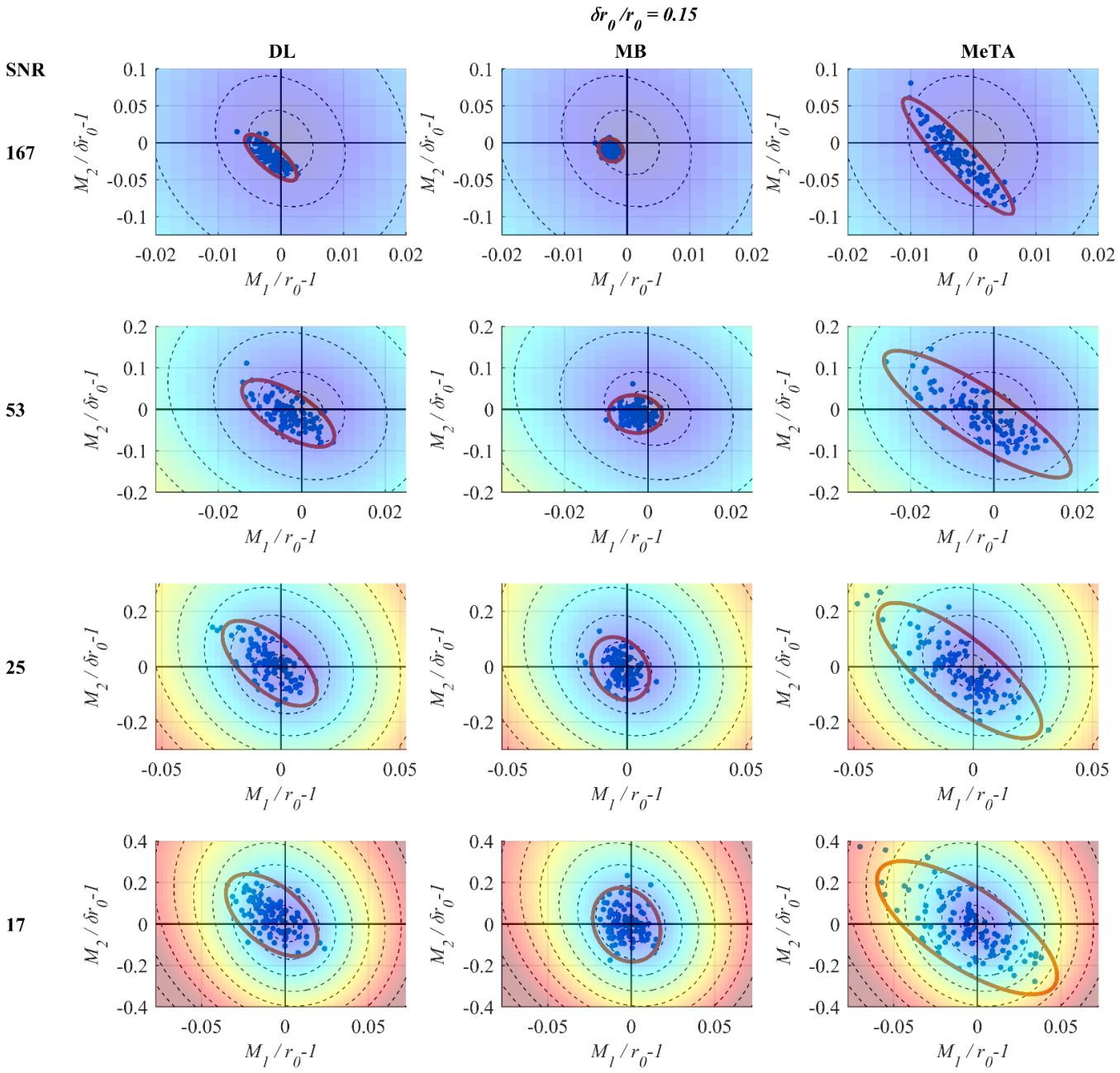

Figure S13. A scatter plot of the relative errors in the M_1 and M_2 values, evaluated by DL (left panels), MB (central panels), and MeTA (right panels) at SNR = 167, 53, 25, and 17 (from top to bottom). The red ellipses show the footprint with the CI=95%. The colored background and dashed lines show the noiseless error-surface. The width of the distance distribution is $\delta r_0/r_0 = 0.15$.

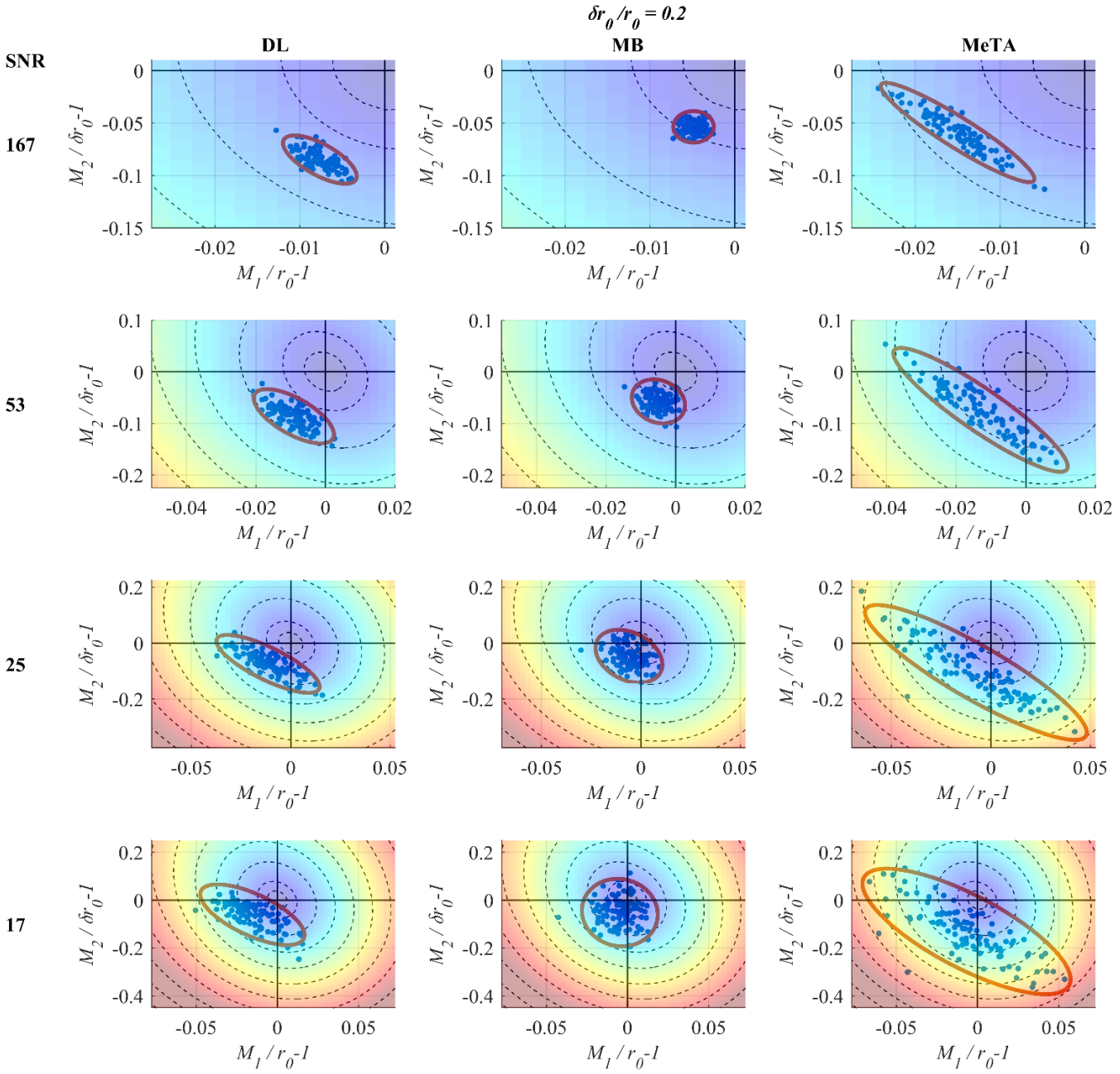

Figure S14. A scatter plot of the relative errors in the M_1 and M_2 values, evaluated by DL (left panels), MB (central panels), and MeTA (right panels) at SNR = 167, 53, 25, and 17 (from top to bottom). The red ellipses show the footprint with the CI=95%. The colored background and dashed lines show the noiseless error-surface. The width of the distance distribution is $\delta r_0/r_0 = 0.2$.

Table S1. Parameters of the confidence ellipses of all datasets for DL, MB, and MeTA. The ellipse parameters characterize the scattered M_1 and M_2 data as follows: the ellipse center is the static bias for M_1 and M_2; the variations are projections of ellipse semiaxis length for the CI=95%. The values for the moments are the relative differences $M_1/r_0 - 1$ and $M_2/\delta r_0 - 1$.

DL		SNR			
$\delta r_0/r_0$		167	53	25	17
0.03	(M_1 bias, M_2 bias)·100%	(-0.09, -0.34)	(-0.27, 0.52)	(-0.66, 4.44)	(-0.68, 9.52)
	(M_1 variation, M_2 variation)·100%	(0.29, 4.46)	(0.84, 7.02)	(1.79, 14.67)	(2.47, 22.33)
0.05	(M_1 bias, M_2 bias)·100%	(-0.06, -0.56)	(-0.22, 0.94)	(-0.36, 5.76)	(-0.75, 11.36)
	(M_1 variation, M_2 variation)·100%	(0.26, 3.46)	(0.93, 9.36)	(1.78, 14.43)	(2.72, 27.04)
0.1	(M_1 bias, M_2 bias)·100%	(-0.06, 0.14)	(-0.19, 2.04)	(-0.41, 7.01)	(-0.56, 11.56)
	(M_1 variation, M_2 variation)·100%	(0.34, 4.31)	(0.96, 8.25)	(1.88, 17.07)	(2.54, 25.11)
0.15	(M_1 bias, M_2 bias)·100%	(-0.16, -2.02)	(-0.33, -0.98)	(-0.47, 1.22)	(-0.81, 4.31)
	(M_1 variation, M_2 variation)·100%	(0.42, 3.12)	(1.11, 8.07)	(1.98, 15.38)	(2.74, 19.82)
0.2	(M_1 bias, M_2 bias)·100%	(-0.76, -8.48)	(-0.91, -8.61)	(-1.14, -7.44)	(-1.54, -6.1)
	(M_1 variation, M_2 variation)·100%	(0.44, 2.3)	(1.15, 5.26)	(2.6, 10.36)	(3.21, 12.68)
MB		SNR			
$\delta r_0/r_0$		167	53	25	17
0.03	(M_1 bias, M_2 bias)·100%	(-0.16, 0.09)	(-0.15, 0.21)	(-0.14, -0.17)	(-0.16, 1.26)
	(M_1 variation, M_2 variation)·100%	(0.07, 2.39)	(0.19, 6.32)	(0.38, 12.46)	(0.60, 21.21)
0.05	(M_1 bias, M_2 bias)·100%	(-0.17, 0.06)	(-0.15, 0.30)	(-0.14, 1.41)	(-0.13, 1.54)
	(M_1 variation, M_2 variation)·100%	(0.09, 2.01)	(0.31, 7.24)	(0.61, 14.10)	(1.00, 24.28)
0.1	(M_1 bias, M_2 bias)·100%	(-0.18, 0.01)	(-0.16, 0.13)	(-0.22, 1.11)	(-0.26, 1.95)
	(M_1 variation, M_2 variation)·100%	(0.15, 2.07)	(0.46, 5.64)	(1.04, 13.57)	(1.53, 20.00)
0.15	(M_1 bias, M_2 bias)·100%	(-0.26, -1.00)	(-0.30, -1.14)	(-0.29, -0.71)	(-0.28, -0.40)
	(M_1 variation, M_2 variation)·100%	(0.20, 1.57)	(0.64, 4.55)	(1.19, 11.40)	(1.99, 17.83)
0.2	(M_1 bias, M_2 bias)·100%	(-0.49, -5.36)	(-0.50, -5.73)	(-0.60, -4.73)	(-0.48, -5.19)
	(M_1 variation, M_2 variation)·100%	(0.24, 1.50)	(0.75, 4.27)	(1.60, 9.50)	(2.33, 14.10)
MeTA		SNR			
$\delta r_0/r_0$		167	53	25	17
0.03	(M_1 bias, M_2 bias)·100%	(-0.02, 2.71)	(-0.07, 6.58)	(-0.08, 9.75)	(-0.02, 10.37)
	(M_1 variation, M_2 variation)·100%	(0.17, 9.75)	(0.5, 31.88)	(0.89, 46.32)	(0.92, 53.02)
0.05	(M_1 bias, M_2 bias)·100%	(-0.01, 3.81)	(-0.05, 7.09)	(-0.02, 11.86)	(-0.11, 11.26)
	(M_1 variation, M_2 variation)·100%	(0.26, 9.05)	(0.65, 22.43)	(1.43, 34.71)	(2.0, 51.24)
0.1	(M_1 bias, M_2 bias)·100%	(0, 0.26)	(-0.05, 2.37)	(-0.02, 3.63)	(0.13, 2.31)
	(M_1 variation, M_2 variation)·100%	(0.43, 6.28)	(1.35, 16.56)	(2.37, 28.49)	(3.55, 32.32)
0.15	(M_1 bias, M_2 bias)·100%	(-0.24, -1.83)	(-0.40, -1.18)	(-0.56, -1.42)	(-0.62, -1.81)
	(M_1 variation, M_2 variation)·100%	(0.88, 7.89)	(2.24, 15.29)	(3.43, 24.47)	(5.39, 32.12)
0.2	(M_1 bias, M_2 bias)·100%	(-1.5, -5.89)	(-1.3, -7.37)	(-0.75, -10.5)	(-0.68, -13.08)
	(M_1 variation, M_2 variation)·100%	(0.91, 4.74)	(2.5, 12.01)	(5.57, 24.12)	(6.4, 26.21)

M_1 and M_2 moment correlations

The M_1 and M_2 and their relative errors are correlated as shown by the tilt of the ellipses noted in the previous section. This correlation is quantified by the ellipse tilt angle, Fig. S15, and by their Pearson correlation coefficients, Fig. S16. The positive counterclockwise angle tilt with respect to the Y-axis shows a negative correlation in M_1 and M_2, i.e., when M_1 is underestimated, M_2 tends to be overestimated. The correlation is small for narrow distributions but is quite noticeable with broad distance distributions.

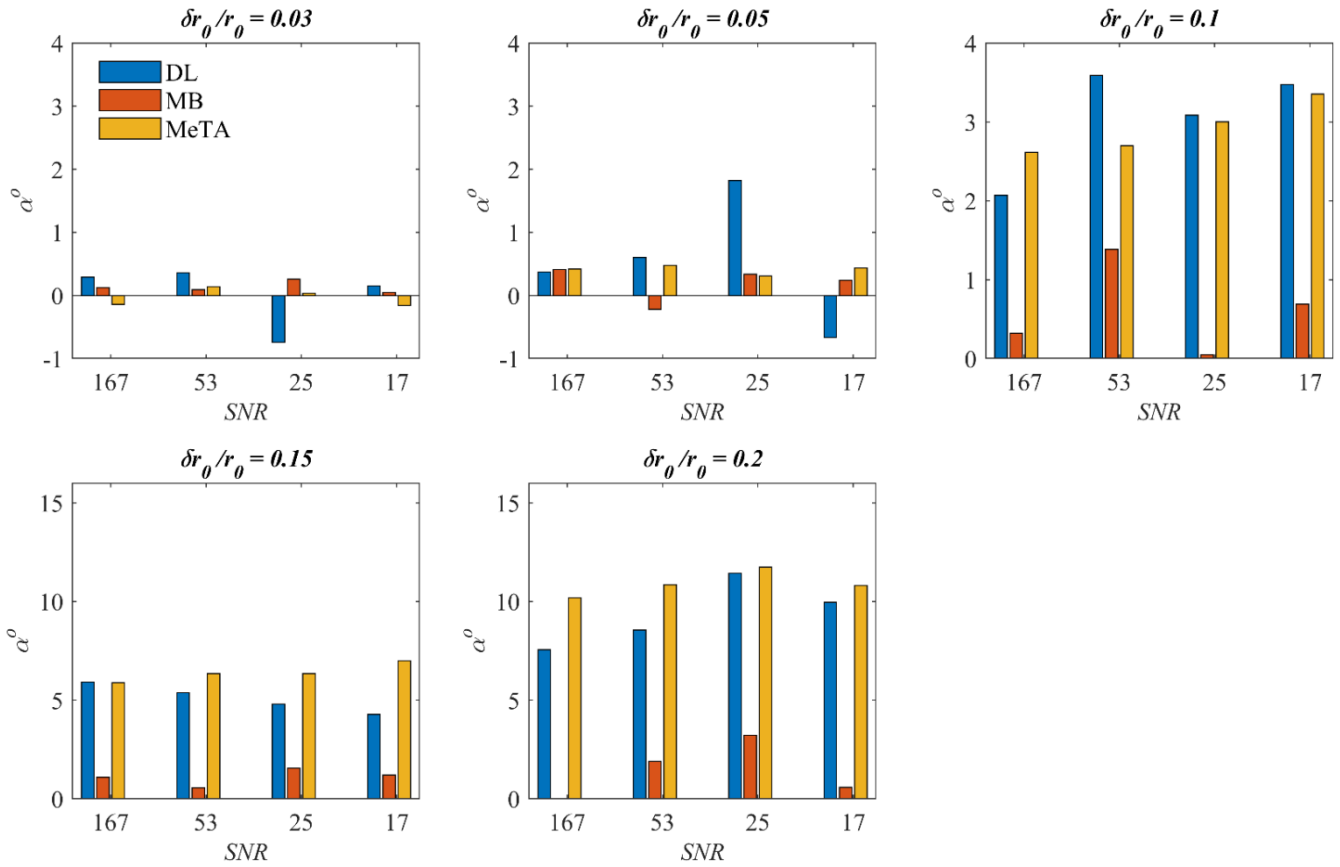

Figure S15. The dependence of the counterclockwise ellipse tilt from the Y-axis (α angle) at different SNR values and different $\delta r_0/r_0$ = 0.03, 0.05, 0.1, 0.15, and 0.2. The color code is the same in all panels.

The Pearson correlation coefficient ρ_{M_1,M_2} reflects the linear correlation in the datasets. A negative weak correlation ρ_{M_1,M_2}< -0.3 is seen for narrow distance distribution functions ($\delta r_0/r_0$=0.03, 0.05), which grows increasingly negative as the DDF broadens, Fig. S16. The Pearson correlation coefficient correlates with the ellipses tilt value, Fig. S15.

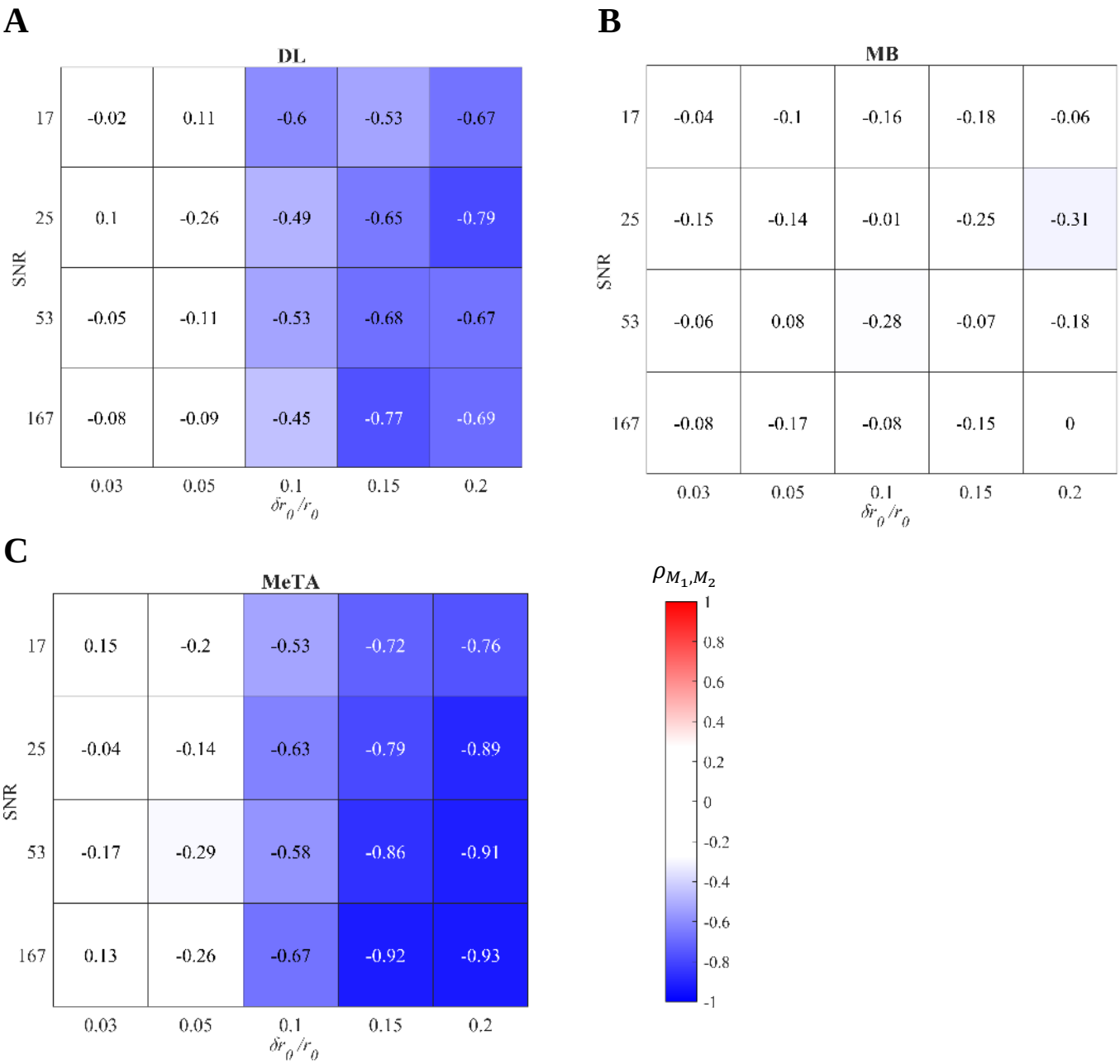

Figure S16. The Pearson correlation coefficient (ρ_{M_1,M_2})for M_1 and M_2 evaluated by DL (**A**), MB (**B**), and MeTA (**C**). The color code for all panels is shown in the color bar.

S6 Migration of the χ^2-surface

The χ^2-surface is the mean square difference between the dipolar traces for the ground truth at r_0, δr_0 and for other r, δr values on the grid with some level of random noise [2]:

$$\chi^2(r, \delta r, \epsilon) = \frac{\sum_i^N \left(V_i^n(r_0, \delta r_0, t_i) + \epsilon(t_i) - V_i^{fit}(r, \delta r, t_i)\right)^2}{\sum_i^N \epsilon(t_i)^2},$$

where N is the total number of experimental points, $V_i^n(r_0, \delta r_0, t_i)$ is the dipolar trace for the ground truth r_0 and δr_0, $\epsilon(t_i)$ is the noise signal which is the same at each position, and $V_i^{fit}(r, \delta r, t_i)$ is the dipolar trace for r and δr. Isolines on the χ^2-surface determine contours, at which the χ^2 is constant.

For convenience, we plot the square root of the χ^2-surface, multiplied by the noise amplitude, which we call the error-surface. Such a plot makes it more convenient to compare the evolving error-surface as the noise amplitude changes using contours from different surfaces.

The "noiseless" error surface was evaluated with no noise, i.e., $\epsilon(t_i) = 0$, Fig. S17, and the remaining surfaces were averaged over 10 independent noise realizations with noise levels corresponding to SNR = 10 - 167 (Fig. S17). For the noiseless surface, the global minimum coincides with the ground truth, i.e., zero bias for both M_1 and M_2. Addition of noise raises the surface above the r_0-dr_0 plane, makes the bottom of the surface blunter, and moves its minimum along an axis connecting the II-IV quadrants, producing a bias for underestimation of M_1 and overestimation of M_2.

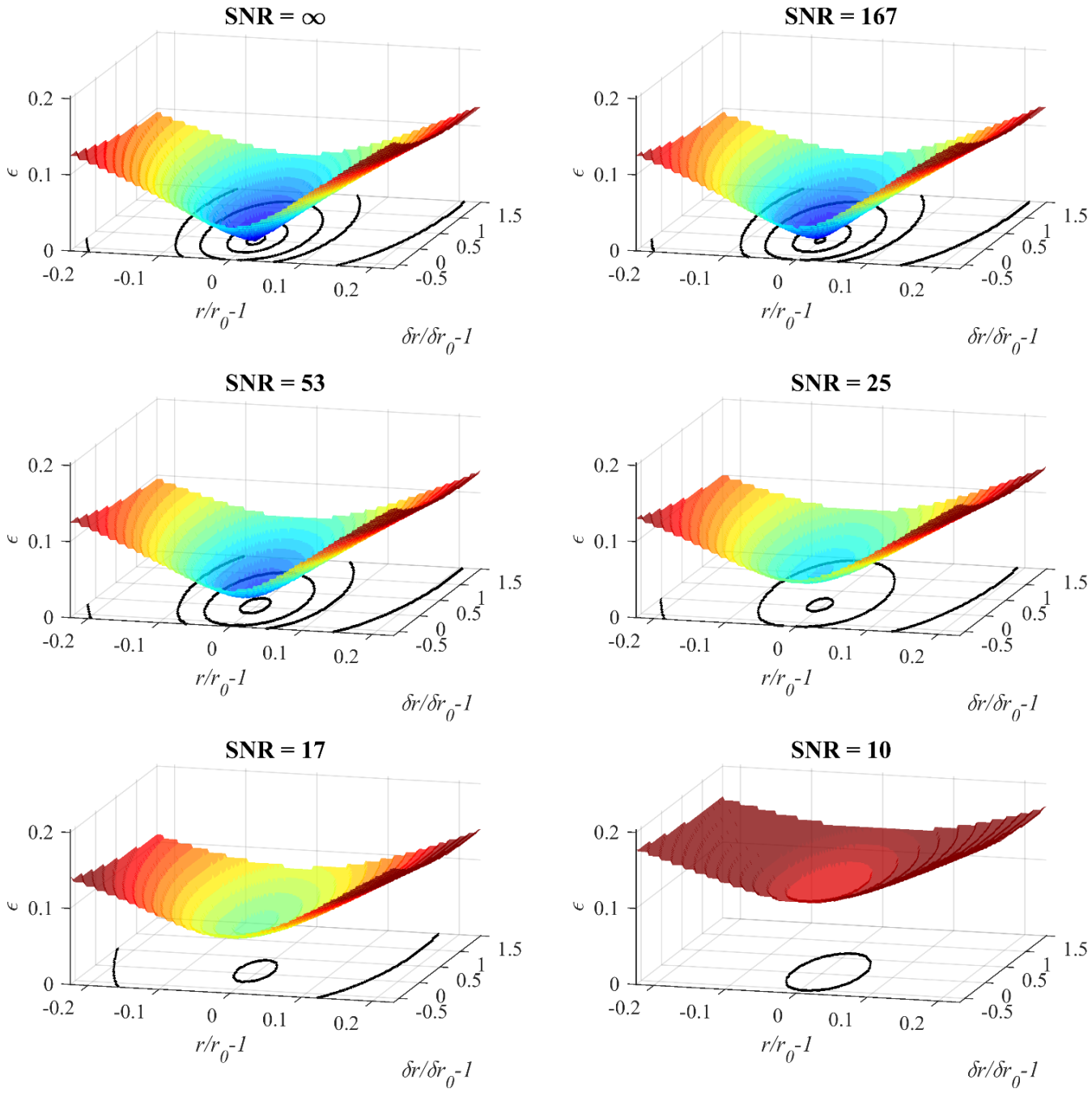

Figure S17. The error-surface at $\delta r_0/r_0$ = 0.1 for the noise-less dipolar trace and averages of 10 random traces with SNR = 167, 53, 25, 17, and 10. Isolines show contours of constant *rmsd* values.

S7 Bias of the "parent" traces and "ascending" datasets

The M_1 and M_2 biases, seen for 'ascending' datasets from traces #17 and #70, Table S2. The biases for the 'ascending' datasets are close to the values of the errors for their 'parent' trace for both DL and MB methods. The ill-posed nature of recovering the distance spectrum is seen in this Table and Figs. 6-7. Traces #17 and #70 have the same ground truth and SNR. Their M_1 and M_2 errors with MB are similar, but with DL rather different. MB and DL give quite different values for the same trace. Each result lies well inside the footprint for the parent dataset of traces #17 and #70. The similarity of the MB values is a random consequence of the ill-posed nature of the problem and not an indication of the quality of the MB approach.

Table S2. The errors and static bias of M_1 and M_2 for the distance spectra recovered by DL and MB approaches for trace #17 and #70 and their "ascending" datasets.

		DL		MB	
		M_1 bias, %	M_2 bias, %	M_1 bias, %	M_2 bias, %
#17	SNR = 25 ("parent" trace)	-1.07	17	-0.20	5.10
	SNR = 20 ("ascending" dataset)	-1.42	21.6	-0.31	5.90
#70	SNR = 25 ("parent" trace)	0.14	2.92	-0.42	1.47
	SNR = 20 ("ascending" dataset)	0.02	2.93	-0.47	0.77

S8 Trends in the confidence bands

The reliability of confidence bands estimated by the bootstrap function of DL was characterized by the fraction of CI=95 bands that fully contain the ground truth within the (r_0-2δr_0, r_0+2δr_0) interval. For 'narrow' DDFs with $\delta r_0/r_0 < 0.1$ the fraction of CI bands that fully include the ground truth is worse than for DDFs with $\delta r_0/r_0 \geq 0.1$ (Table 1). The typical CI bands from a 'narrow' ($\delta r_0/r_0 = 0.05$, trace #43 as an example) versus a 'wide' ($\delta r_0/r_0 = 0.15$, trace #29 as an example) DDF at the same SNR shows some noticeable differences. The 'narrow' distance spectrum has a narrow, thin band whose peak just misses the ground truth, Fig. S18 A. In contrast, the 'wide' distance spectrum has a wider, thicker band which fully includes the ground truth, Fig. S18 B, even though the peaks are somewhat shifted. This example demonstrates how, despite the insignificant bias of trace #43 (-0.0017, 0.0111), the CI band can exclude the part of ground truth, yet for trace #29 with larger biases of (-0.0111, 0.0810), the CI band can fully contain the ground truth.

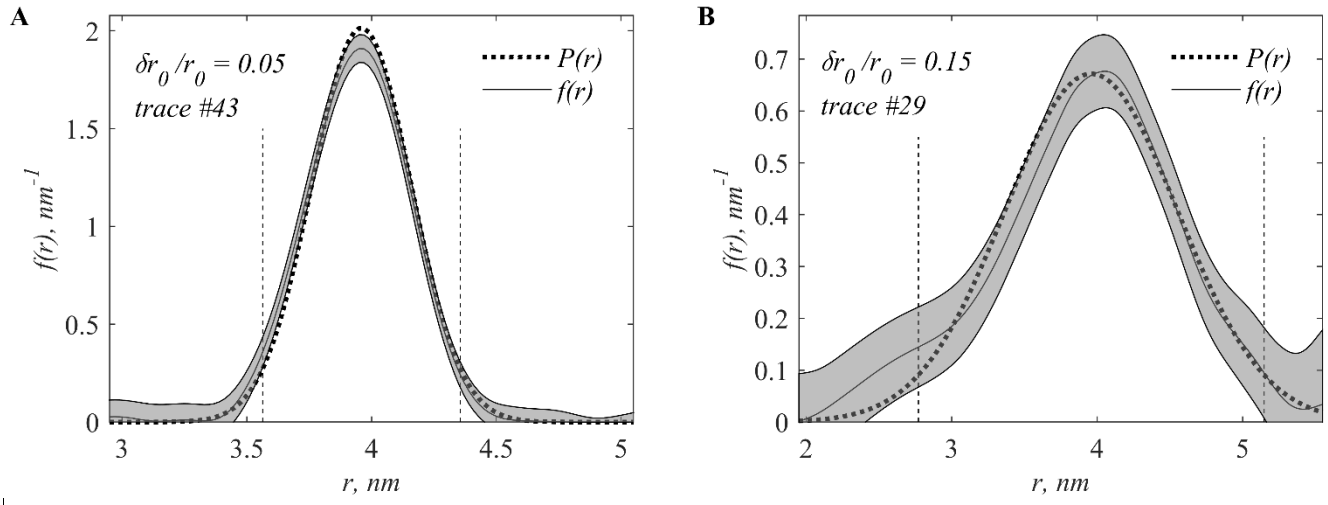

Figure S18. An example of 'narrow' ($\delta r_0/r_0 = 0.05$, **A**) and 'wide' ($\delta r_0/r_0 = 0.15$, **B**) distance spectra (solid curves) and their CI=95 band (grey bands) at SNR = 25. The ground truths are shown by dotted curves, vertical dashed lines show (r_0-2δr_0, r_0+2δr_0) range.

We also examined the mean width or thickness of the CI bands for each dataset as measured as an averaged difference in upper and lower boundaries of the CI=95 band, Fig. S19. For ‘narrow’ DDFs the CI band width is about 1.5-3 times narrower than the band width of the ‘wide’ DDFs.

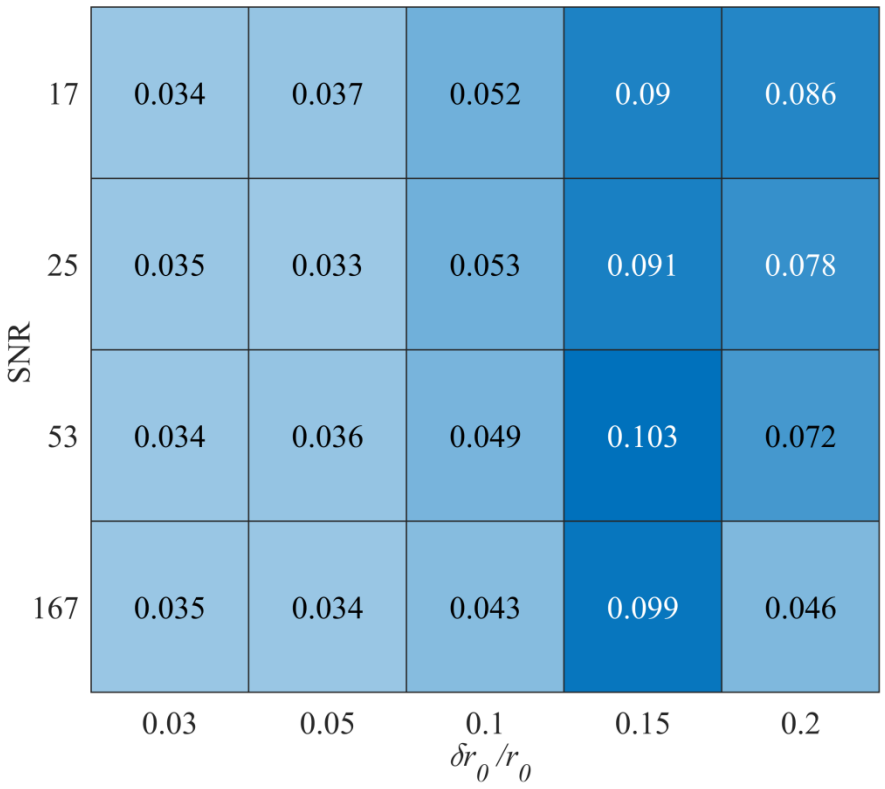

Figure S19. The mean width or thickness of the confidence band (nm^{-1}) for each dataset as measured as an averaged difference in upper and lower boundaries of the CI=95 band.

References

1 A. G. Matveeva, V. N. Syryamina, V. M. Nekrasov and M. K. Bowman, Non-uniform sampling in pulse dipolar spectroscopy by EPR: The redistribution of noise and the optimization of data acquisition, *Phys. Chem. Chem. Phys.*, 2021, **23**, 10335–10346.

2 S. Brandon, A. H. Beth and E. J. Hustedt, The global analysis of DEER data, *J. Magn. Reson.*, 2012, **218**, 93–104.

3 O. Schiemann, C. A. Heubach, D. Abdullin, K. Ackermann, M. Azarkh, E. G. Bagryanskaya, M. Drescher, B. Endeward, J. H. Freed, L. Galazzo, D. Goldfarb, T. Hett, L. Esteban Hofer, L. Fábregas Ibáñez, E. J. Hustedt, S. Kucher, I. Kuprov, J. E. Lovett, A. Meyer, S. Ruthstein, S. Saxena, S. Stoll, C. R. Timmel, M. Di Valentin, H. S. McHaourab, T. F. Prisner, B. E. Bode, E. Bordignon, M. Bennati and G. Jeschke, Benchmark Test and Guidelines for DEER/PELDOR Experiments on Nitroxide-Labeled Biomolecules, *J. Am. Chem. Soc.*, 2021, **143**, 17875–17890.

4 A. G. Matveeva, V. M. Nekrasov and A. G. Maryasov, Analytical solution of the PELDOR inverse problem using the integral Mellin transform, *Phys. Chem. Chem. Phys.*, 2017, **19**, 32381–32388.